Chemistry–A European Journal
Research Article
doi.org/10.1002/chem.202400024
Chemistry Europe
European Chemical Societies Publishing
www.chemeurj.org

Central Ring Puckering Enhances the Stokes Shift of Xanthene Dyes

David Dunlop,[a, b] Peter Horváth,[c] Petr Klán,[c, d] Tomáš Slanina,*[a] and Peter Šebej*[d]

Small-molecule dyes are generally designed based on well-understood electronic effects. However, steric hindrance can promote excited-state geometric relaxation, increasing the difference between the positions of absorption and emission bands (the Stokes shift). Accordingly, we hypothesized that sterically induced central ring puckering in xanthene dyes could be used to systematically increase their Stokes shift. Through a combined experimental/quantum-chemical approach, we screened a group of (9-acylimino)-pyronin dyes with a perturbed central ring geometry. Our results showed that an atom with sp^3 hybridization in position 10 of (9-acylimino)-pyronins induces central ring puckering and facilitates excited-state geometric relaxation, thereby markedly enhancing their Stokes shifts (by up to ~2000 cm^{-1}). Thus, we prepared fluorescent (9-acylimino)-pyronin pH sensors, which showed a Stokes shift disparity between acid and base forms of up to ~8700 cm^{-1}. Moreover, the concept of ring puckering-enhanced Stokes shift can be applied to a wide range of xanthene analogues found in the literature. Therefore, central ring puckering may be reliably used as a strategy for enhancing Stokes shifts in the rational design of dyes.

Introduction

Fluorescent dyes are commonly used for imaging in molecular biology, medicine, neuroscience, and materials science.[1] Their photophysical and chemical properties can be tuned by targeted substitution to enhance their performance in specific applications.[2] In particular, functional dyes are designed to respond to external physico-chemical stimuli through changes in their absorption and emission spectra or even through fluorogenesis and fluorescence quenching.[3]

The ability of functional dyes to meet specific criteria determines the scope and limitations of their applications. For example, a dye which undergoes reversible (de)protonation can be used as a pH sensor, on the condition that its acid-base pair can be spectroscopically resolved.[4] To improve the resolution, the dye should meet two general requirements, namely having (i) sharp absorption and emission bands and a (ii) large Stokes shift.[5] These two properties prevent self-quenching and enable multi-channel imaging, i.e., excitation and detection in two or more different regions of the visible spectrum, and thus, help to spectroscopically resolve each functional form of the dye, or even multiple concurrently applied dyes. Therefore, developing bottom-up approaches to narrow the bandwidth of absorption and emission bands and to tune the Stokes shifts is crucial for applications requiring high resolution, most notably in multi-color imaging techniques.[1b,2a,5–6]

The large Stokes shifts of many dyes have been attributed to geometric relaxation in their excited states.[7] Their excited-state geometric relaxation is facilitated by their vibrational and rotational degrees of freedom.[7c] In turn, these degrees of freedom are increased when introducing rotatable functional groups or molecular fragments,[7b,8] and flexible vibronic backbones.[6b,d,9] Yet, in our previous work,[7a] we have shown that pyronin derivatives with an excocyclic double bond in positon 9 also exhibit a considerably large Stokes shift despite having none of the aforementioned features. Since then, these compounds have been utilized in imaging techniques, most notably by Hell and colleagues in transfection-free multicolor nanoscopy.[10] But while the authors demonstrated the utility of these dyes in imaging applications, the understanding of the origin of their large Stokes shift remains limited, thus preventing further improvements.

Most known dyes absorb light in the visible region due to their extensive π-conjugation, allowing low-energy π–π* transitions.[1a,2c] Yet, the strong spatial overlap between π- and π*-orbitals results in strongly coupled ground and excited states, leading to a small Stokes shift. Due to the strong coupling, manipulating the π-system of these compounds concurrently shifts both absorption and emission bands but does not increase the Stokes shift (Figure 1).[11] By contrast, the large Stokes shift in our dyes is caused by the lack of extended

[a] D. Dunlop, T. Slanina
Institute of Organic Chemistry and Biochemistry of the Czech Academy of Sciences, Flemingovo náměstí 542/2, Prague 6, 160 00 Czech Republic
E-mail: tomas.slanina@uochb.cas.cz
[b] D. Dunlop
Department of Inorganic Chemistry, Faculty of Science, Charles University, Hlavova 2030, Prague 2, 128 40, Czech Republic
[c] P. Horváth, P. Klán
Department of Chemistry, Faculty of Science, Masaryk University, Kamenice 5, 625 00 Brno, Czech Republic
[d] P. Klán, P. Šebej
RECETOX, Faculty of Science, Masaryk University, Kamenice 5, 625 00, Brno, Czech Republic
E-mail: sebej@recetox.muni.cz

Supporting information for this article is available on the WWW under https://doi.org/10.1002/chem.202400024

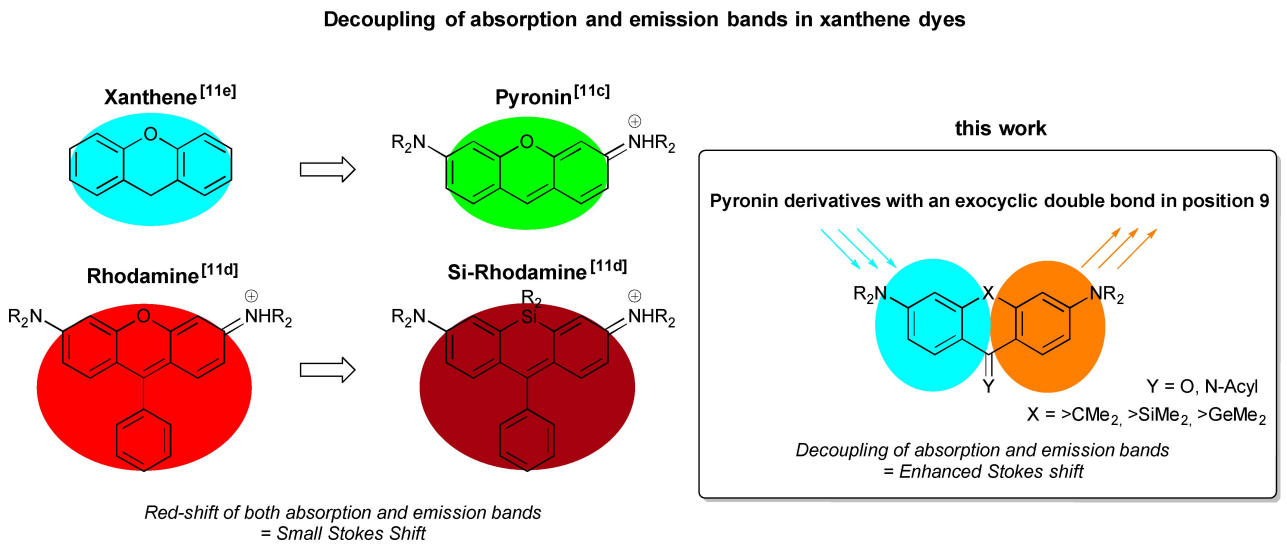

Figure 1. Comparison between previously studied strategies for red-shifting absorption and emission bands in xanthene dyes and the molecular design used in the current study for decoupling the ground and excited states to increase the Stokes shift (the colored fields match the colors of the absorption and emission bands of each compound).[11c–e]

π-conjugation, which precludes π–π* transitions in the visible region. Instead, the electronic transitions of these dyes have a strong charge-transfer (CT) character, thereby allowing decoupling of their ground and excited states by excited-state geometric relaxation.[7a] As such, these compounds provide us with the opportunity to introduce a well-defined, new degree of freedom towards systematically tuning the Stokes shift.

Considering the above, we aimed at developing a general strategy for increasing the Stokes shifts of xanthene dyes by exploiting a geometric feature they all share, that is, by sterically inducing central ring puckering. For this purpose, we studied the photophysical and acid-base properties of a previously developed library of (9-oxo)- and (9-acylimino)-pyronin derivatives bearing –O–, $–C(CH_3)_2–$, $–Si(CH_3)_2–$ and $–Ge(CH_3)_2–$ bridging groups in position 10.[7a,12] Introducing sp^3-hybridized bridging groups to position 10 of the pyronin scaffold alleviated the planarity of its tricyclic core, thereby systematically increasing the Stokes shift. Consequently, the increase of Stokes shift can be directly related to the isomerization energy between the planar and puckered conformations of dyes.

Results and Discussion

We synthesized (9-acylimino)-pyronins **2a–d** and **2a'** from xanthenones **1a–d** and **1a'**, as previously described,[7a,12–13] in a short, high-yielding reaction sequence (Figure 2A–B), consisting of (1) triflation of the ketone moiety, (2) subsequent nucleophilic substitution of triflate for ammonia and (3) *N*-acylation (see Materials and Methods and Supporting Information for details). The nitrogen-linked group in position 9 of **2a–d** and **2a'** was readily protonated in protic solvents, yielding a mixture of acid-base forms, the cationic acid or form A (minor) and the neutral base or form B (major) (Figure 2A). By UV-Vis absorption-emission spectroscopy, we found that the Stokes shift increased in forms B of **1a–d** and **2a–d** when substituting the

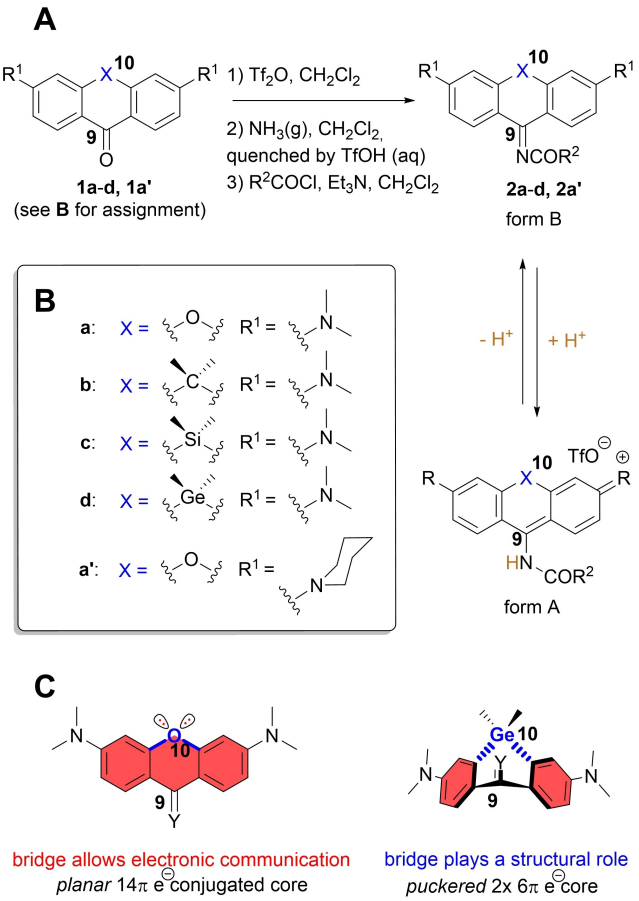

Figure 2. A) Synthesis of (9-acylimino)-pyronins **2a–d** and **2a'**, $R_2 = CH_3$; B) Functional groups in **1a–d**, **2a–d** and **1a'**, **2a'**; and C) Effect of the bridging group X on the molecular geometry of the tricyclic core in form B

sp^2- for sp^3-hybridized bridging groups X (see Table 1 for a complete photophysical characterization of all compounds).

Central Ring Puckering Increases the Excited-State Geometric Relaxation of Only Form B

Form B of **1a** and **2a** has a planar, 14π-e^- tricyclic heteroaromatic core. Nevertheless, their first excited singlet state (S_1) has a strong charge transfer (CT) character, as shown by the calculated charge transfer (D_{CT}) indices (Table S8). This CT does not significantly interfere with the aromaticity of the tricyclic core in S_1. For this reason, the relaxed S_1 geometry of **1a** and **2a** remains planar (see S_0 vs. S_1 geometry comparison in Supporting information (SI), Table S3), and thus the Stokes shifts of these pyronins predominantly derive from the S_1 CT character and relaxation of the bond length and from the bond order of the position 9 substituent. These results corroborate the findings of our previous study.[7a]

To assess whether extending the geometric relaxation of pyronins to their tricyclic core further enhanced their Stokes shifts, the –O– bridging group in position 10 was substituted for sp^3-hybridized, group 14 element-containing $–C(CH_3)_2–$, $–Si(CH_3)_2–$ and $–Ge(CH_3)_2–$ groups (**2b–d**, Figure 2B). Upon this substitution, the previously conjugated 14π-e^- tricyclic core in **1a** and **2a** collapsed into two bridged 6π-e^- rings in **1b–d** and **2b–d** (Figure 2C), as confirmed by our calculations of the electron delocalized density in bonds (EDDB) (see Figure 3A for illustration and SI, Chapter S10, for full EDDB results). This substitution enabled some molecules to adopt a puckered conformation (for an overview of all optimized geometries, see SI, Chapter S7).

We examined the impact of the bridging group on dye geometry using a thorough computational protocol, which involved: (i) conformational sampling (see SI, Chapter S5), subsequent (ii) ground state geometry optimization of the lowest-energy conformers (see SI, Chapter S7 for an overview of all optimized geometries) and (iii) screening of the pathways between the optimized ground-state minimum-energy geometries of model compounds (**m2a–d**, Figure S66) using the nudged elastic band (NEB) method (see SI, Chapter S5 for details on the method and Chapter S8 for the complete results).

Using this protocol, we confirmed that introducing sp^3 hybridized bridging groups to 9-xanthenones **1b–d** increasingly distorted the ground state minimum-energy geometries of their tricyclic cores, albeit preserving their planarity. However, the sp^3 hybridized bridging groups in 9-iminopyronin **2b** allowed planar and puckered ground state minimum-energy geometries. In 9-iminopyronins **2c–d**, the sterically demanding $–Si(CH_3)_2–$ and $–Ge(CH_3)_2–$ bridging groups exclusively enforced the puckered, ground-state, minimum-energy geometries. Moreover, **1b–d** and **2b–d** showed butterfly-like puckering in relaxed S_1 geometries (Table S3).

The S_1 state of **1b** had both planar and puckered minimum-energy geometries, but **1c–d** and **2b–d** were exclusively puckered (Table S3, and SI, Chapter S7). The increased puckering in S_1 of **1c–d** and **2b–d** indicated by our calculations was supported by their UV-Vis spectra (Figure 3B and Table 1). The UV-Vis absorption band maxima varied within a narrower range (~10 nm) in **1b–d** and **2b–d** than in **1a** and **2a**. However, their emission bands were red-shifted by up to ~90 nm. In **2b–d**, in particular, both the UV-Vis emission band maxima and Stokes shifts increased systematically with the atomic radius of the central atom of the bridging group (Table 1). Therefore, we analyzed this relationship in **2b–d** in depth by performing excited-state dynamics simulations of absorption and emission spectra (Figure 3C; see Materials and Methods and SI, Chapter S5, for more methodological details).

The experimentally determined Stokes shift increased with the steric hindrance of the bridging groups in **2b–d**. Rather

Table 1. Spectroscopic Properties of **1a–1d**, **1a'** and **2a–2d**, **2a'** in Methanol.[a]

Compd[b]	Native Form[c]	λ_{abs}^{max}/nm	log ε[d]	λ_{em}^{max}/nm	$\Delta\tilde{\nu}$/cm^{-1} [e]	Φ_f	pK_a[f]
1a'	B	382[g]	4.53[g]	448[g]	3857[g]	0.38 ± 0.01	n.a.[h]
1a	B	379[i]	4.63[i]	442[i]	3761[i]	0.56 ± 0.03[i]	n.a.[h]
1b	B	391	4.59	488	5084	0.60 ± 0.05	n.a.[h]
1c	B	402[i]	4.51[i]	489[i]	4426[i]	0.40 ± 0.03[i]	n.a.[h]
1d	B	399	4.42	490	4654	0.29 ± 0.01	n.a.[h]
2a'[j,k]	B	377	4.50	526	7514	0.17 ± 0.01	7.76 ± 0.20
2a[j,k]	B	376[i]	4.32[i]	513[i]	7103[i]	0.36 ± 0.01[i]	7.61 ± 0.08
2b[j,k]	B	385	4.40	567	8337	0.44 ± 0.01	7.79 ± 0.06
2c[j,k]	B	387[i]	4.24[i]	597[i]	9089[i]	0.56 ± 0.04[i]	6.77 ± 0.06[l]
2d[j,k]	B	383	4.27	589	9132	0.23 ± 0.01	7.14 ± 0.06

[a] Solutions in methanol: c(dye) = 8×10^{-6}–1×10^{-4} mol dm^{-3}. $A(\lambda_{max}) \approx 1$ was adjusted for absorption spectroscopy and $A(\lambda_{max}) < 0.1$ for emission spectroscopy and fluorescence quantum yield measurements; all experiments were performed at 22 °C. [b] Structures shown in Figures 2A and 2B. [c] Acid–base forms (Figure 2A). [d] log [ε/mol dm^{-3} cm^{-1}]. [e] Stokes shifts. [f] All pK_a values were spectrophotometrically determined in an aqueous solution (I = 0.1 mol dm^{-3}, KCl; 1% DMSO (v/v) as cosolvent) and averaged from 2 independent titrations. [g] Data retrieved from Štacko, P. *et al.* (2012).[13b] [h] Not applicable. [i] Data retrieved from Horváth, P. *et al.* (2015).[7a] [j] Data retrieved from Horváth, P. *et al.* (2019).[12] [k] An NaOH (**2a'**) or KOH (**2a–d**) solution was added to the mixture (c_{base} = 1×10^{-3} mol dm^{-3}) to convert form A to form B (Figure 2). [l] Determined for analogous *N*-(3,7-bis(dimethylamino)-5,5-dimethyldibenzo[b,e]silin-10(5*H*)-ylidene-2-(2-(2-methoxyethoxy)ethoxy)acetamide.[7a]

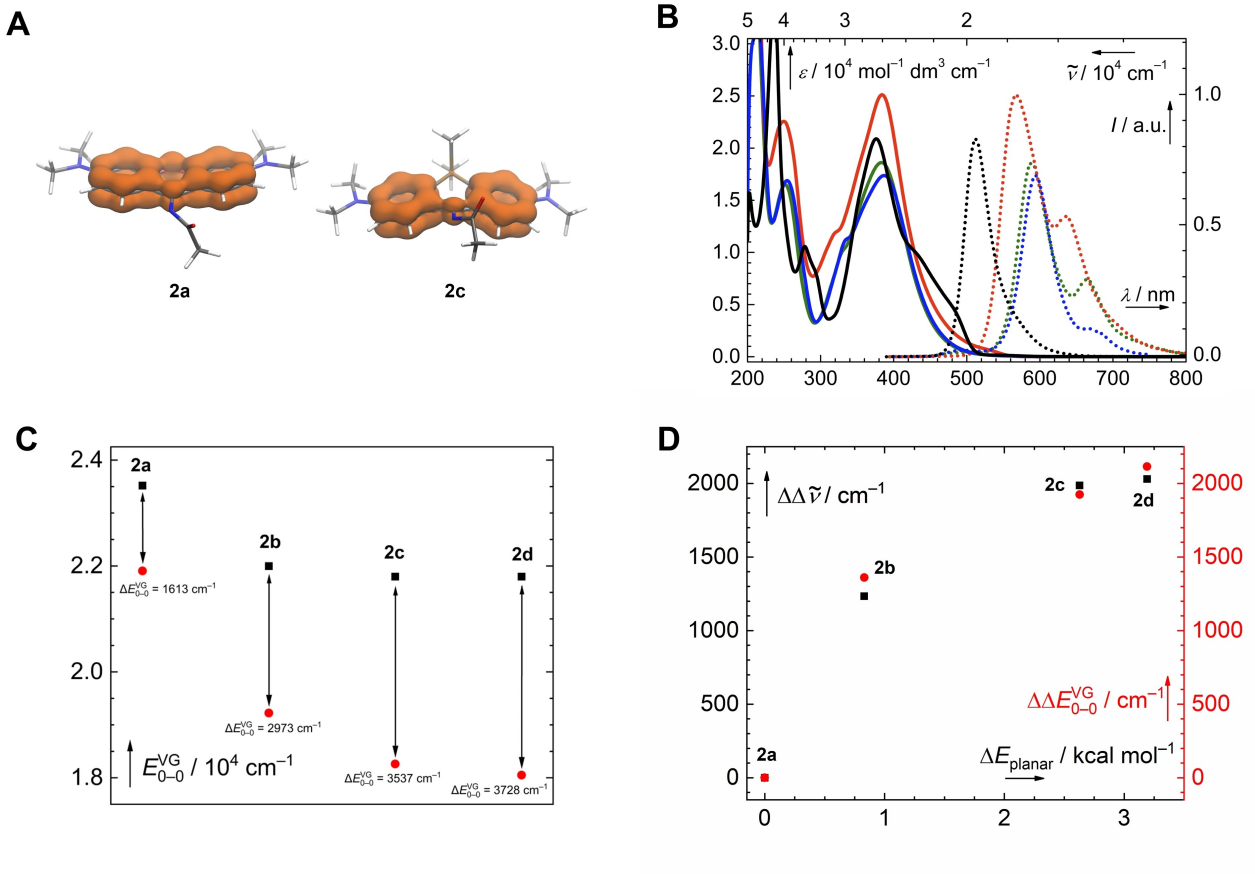

Figure 3. (A) Calculated electron delocalized density in bonds ($EDDB_E$) plots for the tricyclic core fragments of **2a** and **2c**; (B) Measured absorption (solid lines) and emission (dot lines) spectra of **2a–d** in methanol (**2a**, black; **2b**, red; **2c**, blue; **2d**, green); (C) Dot plot of the calculated 0–0 transitions of **2a–d** before (black square) and after (red circle) S_1 relaxation, using a vertical gradient approximation; (D) Dot plot of measured (black square) and calculated (red circle) ring puckering-enhanced Stokes shift in **2a–d** ($\Delta\Delta$ is referenced to the Stokes shift/$\Delta E_{0-0}{}^{VG}$ of planar **2a**) as a function of the energy difference between planar and puckered geometries.

than by stationary geometric parameters, we assessed the steric hindrance by calculating the relative energies of planar vs. puckered geometries of the tricyclic cores (Figure 3D) because these relative energies provide a single-value descriptor of the dynamic behavior of dyes in solution. Moreover, the changes in the measured Stokes shift were virtually equal to the separation of the 0–0 transitions calculated before and after S_1 geometric relaxation (Figure 3C), showing excellent correlation between the S_1 geometric relaxation and the Stokes shift.

The correlation between our calculated and measured data demonstrate a direct, proportional relationship between the increase in Stokes shift and the increase in S_1 geometric relaxation with central ring puckering induced by substitution. As such, central ring puckering is a reliable method for controlling Stokes shifts in (9-imino)-pyronin dyes, in their base form (B).

Electronic Structure of Acid Form Alleviates All Stokes Shifts

Because the acid–base equilibrium of **2a–d** can be reversibly changed by adding strong mineral acids or bases (e.g., HCl or NaOH) to their methanol solutions (Figure 2A), we were able to characterize each form separately (Figure 4B, Table S1). The forms A of **2a–d** showed significantly smaller Stokes shifts (Figure 4B and Table S1) than their neutral counterparts, forms B, due to two, easily rationalized, concurrent effects.

First, protonation of **2a–d** results in the loss of the double bond character of the exocyclic bond in position 9 (Figures 2A and 4A), preventing its geometric relaxation required for a large Stokes shift (as shown by comparing the calculated D_{CT} values of A and B forms of **2a–d**, Table S8). Second, the tricyclic core of cationic **2a–d** forms A adopted a *twisted plane* geometry owing to the recovery of the extended π-system along the tricyclic backbone (Figure 4; for a full overview of the optimized form A ground-state geometries, see Chapter S7.3). In the first excited state, the dyes retained this *twisted plane* geometry (based on S_1 optimized geometries; see Table S3 or Chapter S7.4), so the vibrational overlap between ground- and excited-state vibrational modes of form A compounds increased, and the propensity for S_1 relaxation decreased. In summary, the ground and first excited state were strongly coupled in the acid forms of these compounds. These effects account for the loss of almost all Stokes shifts in all form A compounds, e.g., from 9132 cm^{-1} in form B to 440 cm^{-1} in form A of **2d** (Table S1). These contrasting photophysical properties

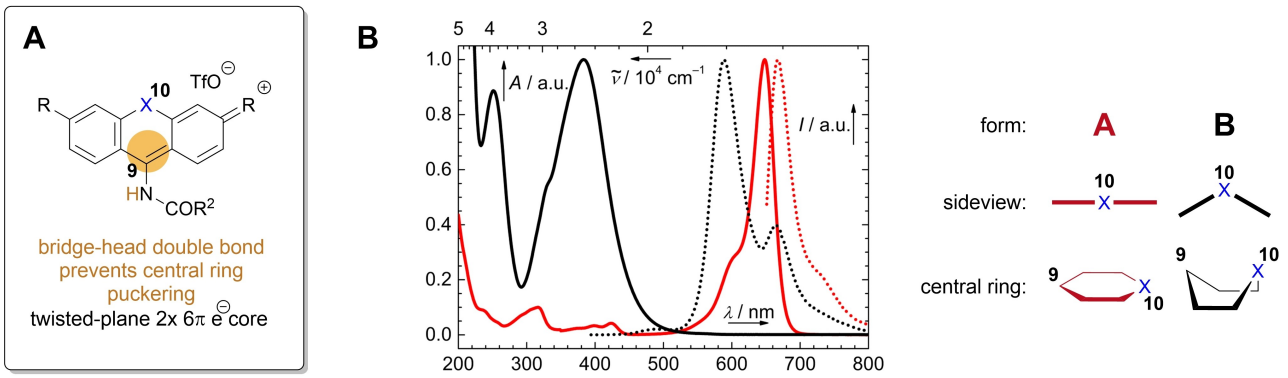

Figure 4. A) Overview of the properties of form A; (B) characteristic UV-Vis spectra of forms A and B (here **2d**) with a color-coded, schematic band assignment (absorption, solid line; emission, dot line; form A red, form B black; sideview along C^9–X^{10} axis)

of acid and base forms experimentally support our proposed structure-property relationship beyond their potential applications in pH-resolved imaging.

Ring puckering-enhanced Stokes shift is a general feature of all xanthene analogues

Stokes shifts result from the separation between ground- and excited-state potential energy surface minima. Accordingly, large Stokes shifts can be induced by S_1 charge transfer character and/or considerable geometric relaxation in the excited state, in any unperturbed single molecule. Moreover, ring puckering-enhanced Stokes shift will, most likely, not be limited to the scaffolds prepared in this study. In fact, this enhancement should also be observed in any puckered xanthene analogue without other inhibiting factors. Below, we briefly overview the literature, which supports this hypothesis.

Only a few examples of puckered xanthene-type dyes, such as those covered herein, have been described so far. The most studied xanthene analogues adopt planar or twisted-plane geometries, enforced by a C9-adjacent bridgehead double bond (analogous to our form A compounds).[3d,6c] This double bond limits their degrees of freedom in both ground and excited states, resulting in strong S_0 and S_1 coupling and, consequently, in a very small Stokes shift. Large Stokes shifts were nevertheless spectroscopically observed in 9-xanthenones and in various position 9-substituted pyronins,[7a,12,14] as well as in structurally related dyes, such as various puckered 9,10-anthraquinone-,[15] phenazine-,[16] and phenothiazine-[17] derivatives.

We also identified a correlation between the Stokes shift and steric hinderance in a series of previously published *meso*-substituted BODIPY dyes, whose tricyclic scaffold is isoelectronic to xanthene's (Figure S2 and Table S2).[18] Attaching methyl groups to different positions of the BODIPY dyes[18a] and substituting fluorine atoms of their BF_2 bridge-group for bulkier alkyl or aryl substituents increasingly facilitated a puckered geometry[18b] and, in turn, increased their Stokes shifts. Although the large number of stable conformers of these compounds hindered our evaluation of their isomerization energies, we calculated the magnitude of central ring puckering in S_0, which correlated well with their relative Stokes shifts (Table S4). These examples indicate that, even in fully conjugated compounds, a similar strategy based on steric hindrance alone can trigger central ring puckering and, hence, increase their Stokes shift.

Moreover, we questioned whether puckered tricyclic compounds analogous to xanthene, but with expanded central rings, would also show a large Stokes shift. For example, dibenzo[b,f]oxepin with a seven-membered central ring and puckered ground-state geometry have a large Stokes shift.[19] Moreover, puckered, tricyclic molecules with 8π-central rings aromatize in the excited state, which leads to large Stokes shifts in other heterocyclic analogues of dibenzo[b,f]oxepin as well, as shown in previous computational studies.[20] These scaffolds were also used to develop complex molecular architectures, such as donor-acceptor dyads[21] and "flapping" perylenediimides.[22]

Based on this brief literature review, the increase in Stokes shift resulting from central ring puckering does not significantly perturb the electronic effects mediated by substituents, as shown by negligible changes in UV-Vis absorption band maxima compared with planar counterparts, where available. However, perturbing dye geometry may increase the rate of non-radiative decay of the excited states, decreasing the fluorescence quantum yield by facilitating low-lying S_1/S_0 conical intersections.[23] Nevertheless, our pyronin-based **1a–d** and **2a–d** are highly tolerant to steric perturbation of their scaffolds (Figure 2C), as confirmed by their high fluorescence quantum yields (Table 1), and by a rudimentary S_1/S_0 conical intersection optimization of planar and puckered model compounds (**m2a** and **m2d**; Figure S71 and S72). No such low-lying conical intersections were computationally observed (conical intersection optimization yielded only isomerization products, which were not experimentally observed either, see SI, Chapter S9). Thus, in xanthene dyes, central ring puckering promotes a significant structural relaxation of the excited-state molecular geometry, thereby increasing the Stokes shift without significantly lowering the high fluorescence quantum yield. This result is exemplified by **2b**, for which we measured fluorescence emission quantum yield of 0.44 ± 0.01 in methanol

(only native form B is present) and 0.59 ± 0.01 in methanol with 1×10^{-3} mol dm^{-3} HCl (see Table S1 for more details).

Conclusions

Central ring puckering of (9-acylimino)-pyronin dyes can be induced by substituting one of the members of the central ring for an sp^3-hybridized $-C(CH_3)_2-$, $-Si(CH_3)_2-$ and $-Ge(CH_3)_2-$ bridging group, triggering a large structural relaxation of their excited state molecular geometry. Geometric relaxation enhances the dyes' Stokes shifts without significantly lowering their fluorescence quantum yields, except when the induced excited-state butterfly modes of the dye facilitate a low-lying S_1/S_0 conical intersection. This strategy is applicable to a wide range of xanthene-type dyes. Overall, our findings demonstrate that central ring puckering of xanthene-type dyes should be considered an essential component of the rational dye design toolkit.

Methods and Materials

Details on preparation, properties and spectral data of dyes **1a'**,[13b] **1a**,[7a] **1b**,[13a] **1c**,[13a] **1d**,[12] **2a'**,[12] **2a**,[7a] **2b**,[12] **2c**[7a] and **2d**[12] are available in SI.

Computational Methods

All quantum chemical calculations were performed using the ORCA 5.0.3 software package.[24] Only D_{CT} indices[25] were calculated by Gaussian 16 rev. C software package.[26] Conformers of each compound were screened in CREST.[27]

Electronic transitions of all compounds were calculated by time-dependent density functional theory (TD-DFT)[28] and STEOM-DPLNO-CCSD[29] calculations (under various constraints), using ground state geometries optimized by density functional theory (DFT)[30] calculations and first singlet excited-state geometries (S_1) optimized by TD-DFT calculations, at B3LYP/def2-TZVP level of theory.[31] Solvent effects were accounted for by C-PCM.[32] Excited state dynamics simulations using the path integral approach[33] were calculated under the vertical gradient approximation. Isomerization trajectories of the conformers were screened by climbing-image nudged elastic band[34] calculations, with subsequent transition state optimization (NEB-TS), disregarding the acyl substituent in **2a**–**d** to avoid contributions of its rotamers (**m2a**–**d**; Figure S66). Energies of all minima and saddle points were refined by a single-point DLPNO-CCSD(T) calculation.[35] S_0–S_1 conical intersections[36] were optimized using a TD-DFT protocol implemented in ORCA 5.0.3, starting from S_1 minimum energy geometries of the **m2a** and **m2d** models, applying first-order non-adiabatic coupling matrix elements[37] and electron translation factors.[38] EDDB plots[39] were calculated using NBO 7.0.[40]

Full technical details on functionals, approximations, and constraints are provided in SI, Chapter S5. All computational results are addressed in SI, Chapters S7–S17.

Supporting Information

The authors have cited additional references within Supporting Information.[41]

Author Contributions

P.Š. conceptualized work with inputs from T.S. and D.D.; D.D. performed the computational study. P.H. synthesized compounds. P.H. and P.Š. measured spectroscopic properties. T.S. supervised work of D.D.; P.K. and P.Š. supervised work of P.H.; D.D. and P.Š. wrote the manuscript with inputs from T.S. All authors approved the final version of the manuscript.

Acknowledgements

This paper is dedicated to the memory of Jakob (Joggi) Wirz. This research was funded by the Czech Science Foundation Grant No. GJ20-30004Y, the Charles University Grant Agency project No. 379321, and the MEYS INTER-COST project No. LTC20076. The authors thank the RECETOX Research Infrastructure (No. LM2023069) financed by the MEYS for supportive background. This work was supported from the European Union's Horizon 2020 research and innovation program under grant agreement No 857560. This publication reflects only the authors' view, and the European Commission is not responsible for any use that may be made of the information it contains. The authors thank Dr. Carlos V. Melo for editing the manuscript. Open Access publishing facilitated by Masarykova univerzita, as part of the Wiley - CzechELib agreement.

Conflict of Interests

There is no conflict to declare.

Data Availability Statement

The data that support the findings of this study are available in the supplementary material of this article.

Keywords: conformation · fluorescence · functional dyes · pyronin · quantum chemical calculations · Stokes shift · xanthene

[1] a) L. D. Lavis, R. T. Raines, *ACS Chem. Biol.* **2014**, *9*, 855–866; b) M. J. Schnermann, *Nature* **2017**, *551*, 176–177; c) R. Strack, *Nat. Methods* **2021**, *18*, 30–30.
[2] a) E. D. Cosco, A. L. Spearman, S. Ramakrishnan, J. G. P. Lingg, M. Saccomano, M. Pengshung, B. A. Arús, K. C. Y. Wong, S. Glasl, V. Ntziachristos, M. Warmer, R. R. McLaughlin, O. T. Bruns, E. M. Sletten, *Nat. Chem.* **2020**, *12*, 1123–1130; b) J. V. Jun, D. M. Chenoweth, E. J. Petersson, *Org. Biomol. Chem.* **2020**, *18*, 5747–5763; c) H. Kuhn, *J. Chem. Phys.* **1949**, *17*, 1198–1212; d) L. D. Lavis, *Annu. Rev. Biochem.* **2017**, *86*,

825–843; e) L. Štacková, E. Muchová, M. Russo, P. Slavíček, P. Štacko, P. Klán, *J. Org. Chem.* **2020**, *85*, 9776–9790.
[3] a) W. Cheng, H. Chen, C. Liu, C. Ji, G. Ma, M. Yin, *VIEW* **2020**, *1*, 20200055; b) S. Kamino, M. Uchiyama, *Org. Biomol. Chem.* **2023**, *21*, 2458–2471; c) S.-H. Kim, *Functional dyes*, Elsevier, **2006**; d) X. Li, X. Gao, W. Shi, H. Ma, *Chem. Rev.* **2014**, *114*, 590–659.
[4] a) J. Han, K. Burgess, *Chem. Rev.* **2010**, *110*, 2709–2728; b) J.-T. Hou, W. X. Ren, K. Li, J. Seo, A. Sharma, X.-Q. Yu, J. S. Kim, *Chem. Soc. Rev.* **2017**, *46*, 2076–2090.
[5] M. V. Sednev, V. N. Belov, S. W. Hell, *Methods Appl. Fluoresc.* **2015**, *3*, 042004.
[6] a) Q. Xu, Y. Zhang, M. Zhu, C. Yan, W. Mao, W.-H. Zhu, Z. Guo, *Chem. Sci.* **2023**, *14*, 4091–4101; b) J. B. Grimm, B. P. English, J. Chen, J. P. Slaughter, Z. Zhang, A. Revyakin, R. Patel, J. J. Macklin, D. Normanno, R. H. Singer, T. Lionnet, L. D. Lavis, *Nat. Methods* **2015**, *12*, 244–250; c) J. B. Grimm, L. D. Lavis, *Nat. Methods* **2022**, *19*, 149–158; d) Y. Miao, N. Qian, L. Shi, F. Hu, W. Min, *Nat. Commun.* **2021**, *12*, 4518.
[7] a) P. Horváth, P. Šebej, T. Šolomek, P. Klán, *J. Org. Chem.* **2015**, *80*, 1299–1311; b) X. Liu, Z. Xu, J. M. Cole, *J. Phys. Chem. C* **2013**, *117*, 16584–16595; c) F. Vollmer, W. Rettig, E. Birckner, *J. Fluoresc.* **1994**, *4*, 65–69.
[8] a) S. Sasaki, G. P. C. Drummen, G.-i. Konishi, *J. Mater. Chem. C* **2016**, *4*, 2731–2743; b) T. Taniguchi, J. Wang, S. Irle, S. Yamaguchi, *Dalton Trans.* **2013**, *42*, 620–624.
[9] a) G. Jiang, T.-B. Ren, E. D'Este, M. Xiong, B. Xiong, K. Johnsson, X.-B. Zhang, L. Wang, L. Yuan, *Nat. Commun.* **2022**, *13*, 2264; b) T.-B. Ren, W. Xu, W. Zhang, X.-X. Zhang, Z.-Y. Wang, Z. Xiang, L. Yuan, X.-B. Zhang, *J. Am. Chem. Soc.* **2018**, *140*, 7716–7722.
[10] A. N. Butkevich, G. Lukinavičius, E. D'Este, S. W. Hell, *J. Am. Chem. Soc.* **2017**, *139*, 12378–12381.
[11] a) C. E. Wheelock, *J. Am. Chem. Soc.* **1959**, *81*, 1348–1352; b) J. Autschbach, *J. Chem. Educ.* **2007**, *84*, 1840; c) B. Yildirim, B. M. Beşer, N. U. Çolak, A. Altay, A. Yaşar, *Biophys. Chem.* **2022**, *290*, 106879; d) Y. Koide, Y. Urano, K. Hanaoka, T. Terai, T. Nagano, *ACS Chem. Biol.* **2011**, *6*, 600–608; e) Y.-H. Tseng, P.-I. Shih, C.-H. Chien, A. K. Dixit, C.-F. Shu, Y.-H. Liu, G.-H. Lee, *Macromolecules* **2005**, *38*, 10055–10060.
[12] P. Horváth, P. Šebej, D. Kovář, J. Damborský, Z. Prokop, P. Klán, *ACS Omega* **2019**, *4*, 5479–5485.
[13] a) T. Pastierik, P. Šebej, J. Medalová, P. Štacko, P. Klán, *J. Org. Chem.* **2014**, *79*, 3374–3382; b) P. Štacko, P. Šebej, A. T. Veetil, P. Klán, *Org. Lett.* **2012**, *14*, 4918–4921.
[14] D. He, L. Zhang, Y. Sun, *Coord. Chem. Rev.* **2022**, *461*, 214507.
[15] J. Yang, A. Dass, A.-M. M. Rawashdeh, C. Sotiriou-Leventis, M. J. Panzner, D. S. Tyson, J. D. Kinder, N. Leventis, *Chem. Mater.* **2004**, *16*, 3457–3468.
[16] Z. Zhang, Y.-S. Wu, K.-C. Tang, C.-L. Chen, J.-W. Ho, J. Su, H. Tian, P.-T. Chou, *J. Am. Chem. Soc.* **2015**, *137*, 8509–8520.
[17] a) C. Arivazhagan, A. Maity, K. Bakthavachalam, A. Jana, S. K. Panigrahi, E. Suresh, A. Das, S. Ghosh, *Chem. Eur. J.* **2017**, *23*, 7046–7051; b) H. Sharma, R. Kakkar, S. Bishnoi, M. D. Milton, *J. Photochem. Photobiol. A* **2022**, *430*, 113944.
[18] a) S. Kim, J. Bouffard, Y. Kim, *Chem. Eur. J.* **2015**, *21*, 17459–17465; b) T. Slanina, P. Shrestha, E. Palao, D. Kand, J. A. Peterson, A. S. Dutton, N. Rubinstein, R. Weinstain, A. H. Winter, P. Klán, *J. Am. Chem. Soc.* **2017**, *139*, 15168–15175.
[19] a) D. Shukla, P. Wan, *J. Am. Chem. Soc.* **1993**, *115*, 2990–2991; b) J. Yan, T. Slanina, J. Bergman, H. Ottosson, *Chem. Eur. J.* **2023**, *29*, e202203748.
[20] a) Y. Chen, S.-M. Tseng, K.-H. Chang, P.-T. Chou, *J. Am. Chem. Soc.* **2022**, *144*, 1748–1757; b) J. Toldo, O. El Bakouri, M. Solà, P.-O. Norrby, H. Ottosson, *ChemPlusChem* **2019**, *84*, 712–721.
[21] G. Sun, Y.-C. Wei, Z. Zhang, J.-A. Lin, Z.-Y. Liu, W. Chen, J. Su, P.-T. Chou, H. Tian, *Angew. Chem. Int. Ed.* **2020**, *59*, 18611–18618.
[22] a) R. Kimura, H. Kuramochi, P. Liu, T. Yamakado, A. Osuka, T. Tahara, S. Saito, *Angew. Chem. Int. Ed.* **2020**, *59*, 16430–16435; b) W. Nakanishi, S. Saito, N. Sakamoto, A. Kashiwagi, S. Yamaguchi, H. Sakai, K. Ariga, *Chem. Asian J.* **2019**, *14*, 2869–2876.
[23] A. Prlj, A. Fabrizio, C. Corminboeuf, *Phys. Chem. Chem. Phys.* **2016**, *18*, 32668–32672.
[24] F. Neese, F. Wennmohs, U. Becker, C. Riplinger, *J. Chem. Phys.* **2020**, *152*, 224108.
[25] T. Le Bahers, C. Adamo, I. Ciofini, *J. Chem. Theory Comput.* **2011**, *7*, 2498–2506.
[26] M. J. Frisch, G. W. Trucks, H. B. Schlegel, G. E. Scuseria, M. A. Robb, J. R. Cheeseman, G. Scalmani, V. Barone, G. A. Petersson, H. Nakatsuji, X. Li, M. Caricato, A. V. Marenich, J. Bloino, B. G. Janesko, R. Gomperts, B. Mennucci, H. P. Hratchian, J. V. Ortiz, A. F. Izmaylov, J. L. Sonnenberg, Williams, F. Ding, F. Lipparini, F. Egidi, J. Goings, B. Peng, A. Petrone, T. Henderson, D. Ranasinghe, V. G. Zakrzewski, J. Gao, N. Rega, G. Zheng, W. Liang, M. Hada, M. Ehara, K. Toyota, R. Fukuda, J. Hasegawa, M. Ishida, T. Nakajima, Y. Honda, O. Kitao, H. Nakai, T. Vreven, K. Throssell, J. A. Montgomery Jr., J. E. Peralta, F. Ogliaro, M. J. Bearpark, J. J. Heyd, E. N. Brothers, K. N. Kudin, V. N. Staroverov, T. A. Keith, R. Kobayashi, J. Normand, K. Raghavachari, A. P. Rendell, J. C. Burant, S. S. Iyengar, J. Tomasi, M. Cossi, J. M. Millam, M. Klene, C. Adamo, R. Cammi, J. W. Ochterski, R. L. Martin, K. Morokuma, O. Farkas, J. B. Foresman, D. J. Fox in *Gaussian 16 Rev. C.01*, *Vol.* Wallingford, CT, **2016**.
[27] P. Pracht, F. Bohle, S. Grimme, *Phys. Chem. Chem. Phys.* **2020**, *22*, 7169–7192.
[28] E. Runge, E. K. U. Gross, *Phys. Rev. Lett.* **1984**, *52*, 997–1000.
[29] A. K. Dutta, F. Neese, R. Izsák, *J. Chem. Phys.* **2016**, *145*, 034102.
[30] W. Kohn, L. J. Sham, *Phys. Rev.* **1965**, *140*, A1133–A1138.
[31] a) A. D. Becke, *J. Chem. Phys.* **1993**, *98*, 5648–5652; b) F. Weigend, R. Ahlrichs, *Phys. Chem. Chem. Phys.* **2005**, *7*, 3297–3305.
[32] M. Garcia-Ratés, F. Neese, *J. Comput. Chem.* **2020**, *41*, 922–939.
[33] B. de Souza, F. Neese, R. Izsák, *J. Chem. Phys.* **2018**, *148*, 034104.
[34] V. Ásgeirsson, B. O. Birgisson, R. Bjornsson, U. Becker, F. Neese, C. Riplinger, H. Jónsson, *J. Chem. Theory Comput.* **2021**, *17*, 4929–4945.
[35] a) Y. Guo, C. Riplinger, D. G. Liakos, U. Becker, M. Saitow, F. Neese, *J. Chem. Phys.* **2020**, *152*, 024116; b) D. G. Liakos, F. Neese, *J. Chem. Theory Comput.* **2015**, *11*, 4054–4063.
[36] S. Maeda, K. Ohno, K. Morokuma, *J. Chem. Theory Comput.* **2010**, *6*, 1538–1545.
[37] Z. Li, W. Liu, *J. Chem. Phys.* **2014**, *141*, 014110.
[38] S. Fatehi, E. Alguire, Y. Shao, J. E. Subotnik, *J. Chem. Phys.* **2011**, *135*, 234105.
[39] D. W. Szczepanik, M. Andrzejak, J. Dominikowska, B. Pawełek, T. M. Krygowski, H. Szatylowicz, M. Solà, *Phys. Chem. Chem. Phys.* **2017**, *19*, 28970–28981.
[40] J. E. D. Glendening, K. Badenhoop, A. E. Reed, J. E. Carpenter, J. A. Bohmann, C. M. Morales, P. Karafiloglou, C. R. Landis, F. Weinhold, in *NBO 7.0*, *Vol.* Theoretical Chemistry Institute, University of Wisconsin, Madison **2018**.
[41] a) H. E. Gottlieb, V. Kotlyar, A. Nudelman, *J. Org. Chem.* **1997**, *62*, 7512–7515; b) G. A. Olah, T. E. Kiovsky, *J. Am. Chem. Soc.* **1968**, *90*, 4666–4672; c) L. Wu, K. Burgess, *Org. Lett.* **2008**, *10*, 1779–1782; d) S. Sugawara, S. Kojima, Y. Yamamoto, *Chem. Commun.* **2012**, *48*, 9735–9737; e) T. Egawa, Y. Koide, K. Hanaoka, T. Komatsu, T. Terai, T. Nagano, *Chem. Commun.* **2011**, *47*, 4162–4164; f) K. Kolmakov, V. N. Belov, C. A. Wurm, B. Harke, M. Leutenegger, C. Eggeling, S. W. Hell, *Eur. J. Org. Chem.* **2010**, *2010*, 3593–3610; g) F. Neese, *Wiley Interdiscip. Rev.: Comput. Mol. Sci.* **2012**, *2*, 73–78; h) F. Neese, *Wiley Interdiscip. Rev.: Comput. Mol. Sci.* **2018**, *8*, e1327; i) C. Adamo, T. Le Bahers, M. Savarese, L. Wilbraham, G. Garcia, R. Fukuda, M. Ehara, N. Rega, I. Ciofini, *Coord. Chem. Rev.* **2015**, *304–305*, 166–178; j) D. W. Szczepanik, M. Solà, in *8 - The electron density of delocalized bonds (EDDBs) as a measure of local and global aromaticity*, (Ed. I. Fernandez), Elsevier, **2021**, pp. 259–284; k) S. Grimme, J. Antony, S. Ehrlich, H. Krieg, *J. Chem. Phys.* **2010**, *132*, 154104; l) S. Grimme, S. Ehrlich, L. Goerigk, *J. Comput. Chem.* **2011**, *32*, 1456–1465; m) R. Izsák, F. Neese, *J. Chem. Phys.* **2011**, *135*, 144105; n) F. Weigend, *Phys. Chem. Chem. Phys.* **2006**, *8*, 1057–1065; o) M. Feyereisen, G. Fitzgerald, A. Komornicki, *Chem. Phys. Lett.* **1993**, *208*, 359–363; p) S. Grimme, A. Hansen, *Angew. Chem. Int. Ed.* **2015**, *54*, 12308–12313; q) C. Bannwarth, S. Ehlert, S. Grimme, *J. Chem. Theory Comput.* **2019**, *15*, 1652–1671; r) M. Garcia-Ratés, F. Neese, *J. Comput. Chem.* **2019**, *40*, 1816–1828; s) S. Grimme, *J. Chem. Phys.* **2006**, *124*, 034108; t) T. Yanai, D. P. Tew, N. C. Handy, *Chem. Phys. Lett.* **2004**, *393*, 51–57; u) W. Humphrey, A. Dalke, K. Schulten, *J. Mol. Graphics* **1996**, *14*, 33–38.

Manuscript received: January 3, 2024
Accepted manuscript online: January 10, 2024
Version of record online: February 15, 2024